LGS AO and MCAO Performance as a Function of LGS Signal Level

Brent Ellerbroek

1 December 1999

1 Introduction and Summary

This note describes the results of a study of LGS AO and MCAO performance as a function of LGS signal level, based upon our present estimates for Cerro Pachon atmospheric parameters and the characteristics of the AO hardware. The LGS signal level requirements for a given Strehl ratio due to the combined effects of noise and servo lag appear to be slightly higher than estimated previously for the Altair LGS upgrade [1], primarily because we have considered an AO system with 16 subapertures across the telescope pupil and have made somewhat more pessimistic assumptions on the diameter of the laser guide star. A WFS signal level of from 80 to 200 photodetection events (PDE's) per square centimeter of collecting area per second still provides an entirely satisfactory level of performance. With 80 photodetection events, for example, the H band Strehl ratio due to the combined effects of noise and servo lag for LGS AO is 0.95 for average seeing and a zero degree zenith angle. For J band the Strehl ratio due to these effects is 0.91, which increases to 0.93 [0.95] with for 125 [200] photodetection event. These last three values also describe performance in H band at a 45 degree zenith angle. Optimized WFS sampling rates for these cases range from about 500 to 800 Hz, but the performance variations with sampling rate and control bandwidth are very slight due to the tradeoff between servo lag and noise gain. The variations in performance between 4 and 6 electrons of detector read noise in the WFS camera are also very modest, with more appreciable penalties for 9 noise electrons.

The Strehl ratio reductions for a given LGS signal level are somewhat more significant for MCAO than for LGS AO. In H band the degradation is greater by 2–3 per cent (absolute) at the center of the MCAO field, and the difference increases to as much as 7–9 per cent at the edge of the field. Heuristically, this increased sensitivity to noise for MCAO may arise from the need to invert the cross-coupled influence of multiple deformable mirrors upon multiple wave front sensors. Even with this increased sensitivity to noise, LGS signal levels in the range of 80 to 200 PDE's/cm^2/sec provide a fairly reasonable level of compensation over a field-of-view much larger than provided by conventional AO.

The results in this report have been derived using analytical models very similar to those previously used for Altair [2]. The Shack-Hartmann WFS model, however, has been upgraded to model the elongation and increased diameter of the Shack-Hartmann WFS spots resulting from the use of LGS AO. The equations used to model the Shack-Hartmann WFS spots are summarized in section 2, and the formulas expressing WFS tilt measurement error as a function spot shape and other parameters are given in section 3. Numerical results on LGS AO performance as a function of LGS signal level for optimized control bandwidths are presented in section 4. Section 5 summarizes MCAO performance for LGS signal levels between 80 and 200 PDE's/cm^2/sec, using the control bandwidths previously optimized for the conventional LGS AO systems.[1] Finally, section 6 reviews the relationship between LGS single level and laser source power, given our current estimates for optical transmittance values and sodium layer characteristics [1].

It is important to note that the LGS AO and MCAO performance estimates in this report do not include the effects of (i) measurement noise for NGS tip/tilt WFS's, and (ii) noncommon path optical aberrations and other calibration error sources. These error sources will be considered in future reports.

[1] Explicit optimization of the control bandwidth for MCAO is beyond the scope of a conceptual design analysis, given the length of time required for each calculation.

2 Modeling LGS Shack-Hartmann Spots

The shape of the LGS spots as detected by the Shack-Hartmann WFS CCD is a function of factors including

- The profile of the outgoing laser beam at the launch telescope;
- The launch telescope aperture diameter;
- Atmospheric turbulence effects on the beam as it propagates up to the sodium layer;
- The vertical distribution of the sodium layer;
- Atmospheric turbulence effects on the return signal as it propagates down to the telescope aperture;
- The width of each WFS subaperture in the telescope aperture plane;
- Aberrations in the Shack-Hartmann WFS lenslet array; and
- Pixel-to-pixel crosstalk in the WFS CCD.

This analysis uses a MTF approach to model these effects, multiplying a transfer function for each of the above terms together to estimate the mean tilt-removed LGS image as detected by the WFS CCD. This is an extension of the method used to model NGS WFS measurement noise for Altair, where only the last four items need be considered [3]. Subsection 2.1 summarizes the formulas used for each transfer function, and subsection 2.2 outlines some of the approximations inherent in using this approach.

2.1 Tranfer function formulas

The transfer-function-based model used for the LGS Shack-Hartmann spot S is given by the equation

$$S = \mathrm{PSF}_T * T_{A,T} * T_E * T_{A,R} * \mathrm{PSF}_R * T_L * T_D, \tag{1}$$

where PSF_T is the far-field pattern corresponding to the laser beam profile at the launch telescope aperture, $T_{A,T}$ is the blurring due to atmospheric turbulence on the transmit path, T_E is the elongation of the image caused by the depth of the sodium layer, $T_{A,R}$ is the blurring due to atmospheric turbulence on the receive path, PSF_R is the diffraction limited far-field pattern for a WFS subaperture, T_L is the blurring due to imperfections in the WFS lenslet array, T_D is the blurring due to crosstalk between the pixels in the CCD array, and "$*$" denotes the convolution operator. Applying the Fourier transform operator to each side of this expression yields

$$\widehat{S} = \widehat{\mathrm{PSF}}_T \widehat{T}_{A,T} \widehat{T}_E \widehat{T}_{A,R} \widehat{\mathrm{PSF}}_R \widehat{T}_L \widehat{T}_D, \tag{2}$$

where $\widehat{f}$ denotes the Fourier transform of the function f. The remainder of this subsection outlines the usual formulas for these transfer functions. Please note that these formulas assume that a factor of 2π is included in the Fourier transform kernal.

In general, the term $\widehat{\mathrm{PSF}}_T$ will be the autocorrelation of the laser beam amplitude and phase profile as transmitted by the laser launch telescope. For the special case of an unaberrated beam with a uniform amplitude profile,

$$\widehat{\mathrm{PSF}}_T(\kappa) = \left(\frac{2}{\pi}\right)\left\{\cos^{-1}\left(\frac{\kappa\lambda}{d_T}\right) - \left(\frac{\kappa\lambda}{d_T}\right)\left[1 - \left(\frac{\kappa\lambda}{d_T}\right)^2\right]^{1/2}\right\}, \tag{3}$$

where κ is an angular spatial frequency variable, λ is the laser wavelength, d_T is the aperture diameter of the launch telescope, and $\kappa\lambda/d_T \leq 1$. For an ideal, untruncated Gaussian laser beam the formula becomes

$$\widehat{\mathrm{PSF}}_T(\kappa) = \exp[-2(\kappa\lambda)^2/d_B^2], \tag{4}$$

where d_B is the full-width, $1/e^2$-maximum of the beam. In this case, the effects of beam quality can be estimated using the approximation

$$d_B = d_{B_0}/\mathrm{BQ}, \tag{5}$$

where d_{B_0} is the diameter of the best-fit Gaussian and BQ is the beam quality for the laser.

The blurring due atmospheric turbulence on the transmit path is modelled using Fried's short exposure formula,

$$\widehat{T}_{A,T}(\kappa) = \exp\left\{-3.44\left(\frac{d_T}{r_0}\right)^{5/3}\left(\frac{\kappa\lambda}{d_T}\right)^{5/3}\left[1-\left(\frac{\kappa\lambda}{d_T}\right)^{1/3}\right]\right\}, \tag{6}$$

where r_0 is the turbulence-induced effective coherence diameter at the laser wavelength. The term within square brackets models the effect of tip/tilt correction using feedback from LGS WFS; with this term removed, the formula reduces to the usual long-exposure transfer function. Similarly, the transfer function for the effect of turbulence on the return path is given by

$$\widehat{T}_{A,R}(\kappa) = \exp\left\{-3.44\left(\frac{d_R}{r_0}\right)^{5/3}\left(\frac{\kappa\lambda}{d_R}\right)^{5/3}\left[1-\left(\frac{\kappa\lambda}{d_R}\right)^{1/3}\right]\right\}, \tag{7}$$

where d_R is the diameter of a WFS subaperture. Note that these formulas were originally derived for uniform amplitude profiles on circular apertures, and approximations are made when they are applied to Gaussian beams or square subapertures as discussed in subsection 2.2 below.

Assuming that the depth of focus for the projected laser beam is longer than the depth of the sodium layer, the elongation of the LGS can be modelled using a one dimensional convolution. For a WFS subaperture separated from the launch telescope by a distance d_s along the x direction, a paraxial approximation to the elongation function $T_E(\theta)$ is given by

$$T_E(\theta_x,\theta_y) \propto \delta(\theta_y)\left[H\left(1+\frac{H\theta_x}{d_s}\right)\right]^{-2}\rho\left(H\left(1+\frac{H\theta_x}{d_s}\right)\right). \tag{8}$$

Here δ is the Dirac delta function, H is the mean range of the sodium layer, and ρ is the density of the sodium layer as a function of range. Unfortunately, this last quantify is too variable to be modelled with any precision by a single function. We therefore adopt the simple tophat approximation

$$T_E(\theta_x,\theta_y) = \begin{cases} \delta(\theta_y)/\Delta & \text{if } \theta_1 \le \theta \le \theta_2, \\ 0 & \text{otherwise,} \end{cases} \tag{9}$$

$$\Delta = \theta_2 - \theta_1, \tag{10}$$

$$\theta_i = \frac{d_s}{H}\left(\frac{H_i}{H}-1\right) \qquad i=1,2, \tag{11}$$

where H_1 and H_2 are ranges to the lower and upper bounds of the sodium layer, and θ_1 and θ_2 are the corresponding angles on the focal plane of the WFS.[2] The corresponding transfer function for a separation d_s along the x axis is given by

$$\widehat{T}_E(\kappa) = \delta(\kappa_y)\frac{\sin(\pi\Delta\kappa_x)}{\pi\Delta\kappa_x}. \tag{12}$$

This function rotates with the direction of the separation between the launch telescope and the WFS subaperture.

Next, the diffraction-limited transfer function for a WFS subaperture of width w is given by

$$\widehat{\mathrm{PSF}}_R(\kappa) = \begin{cases} \left(1-\left|\frac{\kappa_x\lambda}{w}\right|\right)\left(1-\left|\frac{\kappa_y\lambda}{w}\right|\right) & \text{for } |\lambda\kappa_x| \le w \text{ and } |\lambda\kappa_y| \le w, \\ 0 & \text{otherwise.} \end{cases} \tag{13}$$

Additional blurring of the subaperture images by imperfections in the lenslet array can be (roughly) approximated by the Gaussian transfer function

$$\widehat{T}_L(\kappa) = \exp\left[-2\pi^2\left(\frac{\kappa\lambda\sigma_L}{w_R}\right)^2\right], \tag{14}$$

[2] Note that these angle (i.e., the amount of elongation) do depend upon the separation d_s between the launch telescope and the subaperture.

where σ_L is the standard deviation of the Gaussian blur expressed as a fraction of the diffraction angle λ/w_R. Finally, the blurring caused by pixel crosstalk in the CCD array can also be represented as the Gaussian transfer function

$$\widehat{T}_D(\kappa) = \exp\left[-2\pi^2 \left(\kappa w_D \sigma_D\right)^2\right]. \tag{15}$$

Here σ_D is the standard deviation of the Gaussian, expressed as a function of the (angular) pixel subtense w_D.

2.2 Approximations in the model

The transfer function for the short-exposure bluring due to atmospheric turbulence is only an approximation, which is reasonably accurate for aperture diameters smaller than 2 or 3 r_0. Further approximation are introduced when it is applied to square subapertures or Gaussian beams. In addition, this transfer function only estimates the mean blurring due to atmospheric turbulence, not measurement-to-measurement fluctuations in the shape of the LGS image. Except for the use of Gaussian beams, all of these approximations were found to have very little effect when analytical predictions were compared against more detailed simulation results for Altair [2].

The use of a tophat function for the density of the sodium layer increases the effects of elongation and yields a conservative estimate for the diameter of the LGS. Since the degree of elongation is fixed, the current model does not incorporate the effects of WFS calibration errors arising from temporal variations in the distribution of the sodium layer. Using the approach described here, we do intend to model the variability in LGS images as a function of changes in sodium layer distribution, and reconstruct these variations into the resulting biases in the estimated wave front.

The additional blurring due to imperfections in the WFS lenslet array should formally be treated coherently with the WFS transfer function $\widehat{\mathrm{PSF}}_R$. For properly fabricated lenslets this term will be small relative to the remaining effects, and no better model is available until a specific lenslet array is selected.

3 WFS Measurement Error Due to Noise

In this section we assume that two by two pixels and the standard quad cell algorithm are used to estimate the local wavefront tilt in each Shack-Hartmann subaperture. The RMS tilt estimation error for this approach is a function of the signal-to-noise ratio and the gain of the quad cell energy imbalance with respect to tilt, which are in turn functions of the shape of the LGS image, the WFS pixel size, and the input signal level. The following paragraphs present the formulas used to evaluate the RMS tilt measurement error and present sample numerical results.

3.1 Summary of Approach

For a LGS image with shape S computed as in the preceeding section, the fraction of the total image signal incident on a particular pixel is given by

$$\frac{\bar{N}_i}{\bar{N}} = \frac{\int dr\, S(r-\theta) D(r-r_i)}{\int dr\, S(r)}, \tag{16}$$

where $\bar{N}$ is the average total number of photodection events in the subaperture, $\bar{N}_i$ is the average number of photodection events on pixel number i, θ is the subaperture wavefront tilt, D is the response function for a pixel centered at the origin of the focal plane, and r_i is the location of pixel number i. The function D will be modelled as a square tophat of width w_p, since the blurring due to pixel crosstalk is already accounted for in the LGS image S as described in section 2 above. Using the Plancheral and shift theorems, the right-hand-side of this expression may be rewritten as

$$\frac{\bar{N}_i}{\bar{N}} = \frac{\int d\kappa\, \widehat{S}(\kappa)\widehat{D}(\kappa) \exp[-2\pi i \kappa \cdot (\theta - r_i)]}{\widehat{S}(0)}, \tag{17}$$

where the Fourier transform of the square tophat detector response function is given by

$$\widehat{D}(\kappa) = \left[\frac{\sin(\pi w_p \kappa_x)}{\pi \kappa_x}\right]\left[\frac{\sin(\pi w_p \kappa_y)}{\pi \kappa_y}\right]. \tag{18}$$

(The complex conjugates which would normally appear in Eq.'s (16) and (17) can be dropped, since both D and $\widehat{D}$ are real valued functions). For a quadrant detector, the location of the pixels in the four quadrants is given by

$$r_j = \sqrt{0.5} w_p (\cos(\pi/4 + j\pi/2), \sin(\pi/4 + j\pi/2)) \tag{19}$$

for $j = 1, \ldots, 4$, and the quad cell energy imbalance in the x-direction is defined by the formula

$$\Delta_x = \frac{N_1 + N_4 - N_2 - N_3}{N_1 + N_2 + N_3 + N_4}. \tag{20}$$

Using Eq. (17), this becomes

$$\Delta_x = \frac{i \int d\kappa\, \widehat{S}(\kappa)\widehat{D}(\kappa) \exp(-2\pi i \kappa \cdot \theta) \cos(\pi w_p \kappa_y) \sin(\pi w_p \kappa_x)}{\int d\kappa\, \widehat{S}(\kappa)\widehat{D}(\kappa) \exp(-2\pi i \kappa \cdot \theta) \cos(\pi w_p \kappa_y) \cos(\pi w_p \kappa_x)}. \tag{21}$$

For the y-energy imbalance Δ_y, the quantities κ_x and κ_y are transposed in the numerator.

The quad cell tilt estimation algorithm is simply

$$\vartheta_x = \left(\left.\frac{\partial \Delta_x}{\partial \theta_x}\right|_{\theta=0}\right)^{-1} \Delta_x, \tag{22}$$

where ϑ is the estimate of the actual tilt θ, and $\partial \Delta_x / \partial \theta_x$ is the gain of the quadrant detector measurement. In the linear range of the quad cell, the mean-square error in the estimate due to noise is given by

$$\begin{aligned} \sigma^2_{\theta_x} &= \left\langle (\vartheta_x - \theta_x)^2 \right\rangle \\ &= \left(\frac{\partial \Delta_x}{\partial \theta_x}\right)^{-2} \left\langle (\Delta_x - \langle \Delta_x \rangle)^2 \right\rangle, \end{aligned} \tag{23}$$

where the angle brackets denote ensemble averages over noise statistics. The terms on the right-hand side of the expression can be computed using Eq.'s (17), (20), and (21) above

The quadrant detector gain is computed by differentiating the right-hand-side of Eq. (21) with respect to θ. The derivative of the denominator with respect to θ will be zero if the function $\widehat{S}$ is real-valued, i.e., if the LGS image S is symmettric. Alternatively, the derivative of the denominator will be small relative to the derivative of the numerator if a large fraction of the total LGS image is incident on the quad cell. Assuming that one of these conditions applies, the quadrant detector gain is equal to (or well approximated by)

$$\left.\frac{\partial \Delta_x}{\partial \theta_x}\right|_{\theta=0} = \frac{2\pi \int d\kappa\, \widehat{S}(\kappa)\widehat{D}(\kappa)\kappa_x \cos(\pi w_p \kappa_y) \sin(\pi w_p \kappa_x)}{\int d\kappa\, \widehat{S}(\kappa)\widehat{D}(\kappa) \cos(\pi w_p \kappa_y) \cos(\pi w_p \kappa_x)}. \tag{24}$$

Once again, the corresponding expression for the y-tilt gain is obtained by transposing κ_x and κ_y in the numerator.

To compute the mean-square variability in Δ_x with respect to noise we assume that (i) the variability in each N_i is due to a combination of photon statistics and detector read noise which is uncorrelated from pixel to pixel, and (ii) the energy imbalance Δ_x is near null, so that the relative variability in the numerator of Eq. (20) is much greater than the relative variability in the denominator. With these assumptions, the mean square variability in Δ_x is given by

$$\left\langle (\Delta_x - \langle \Delta_x \rangle)^2 \right\rangle = \frac{\bar{N}_1 + \bar{N}_2 + \bar{N}_3 + \bar{N}_4 + 4B + 4\sigma_e^2}{(\bar{N}_1 + \bar{N}_2 + \bar{N}_3 + \bar{N}_4)^2}, \tag{25}$$

where B is the average number of background photodetection events per pixel, and σ_e is the RMS number of read noise electrons per pixel per read. It convenient to define f as the fraction of the total subaperture signal level which is detected by the quad cell, i.e.

$$f = \frac{\bar{N}_1 + \bar{N}_2 + \bar{N}_3 + \bar{N}_4}{\bar{N}}. \tag{26}$$

The mean-square variability in Δ_x can then be expressed as

$$\left\langle (\Delta_x - \langle \Delta_x \rangle)^2 \right\rangle = \frac{f\bar{N} + 4B + 4\sigma_e^2}{(f\bar{N})^2}. \tag{27}$$

Using Eq. (17), the fraction f may be evaluated as

$$f = \frac{4 \int d\kappa \, \widehat{S}(\kappa) \widehat{D}(\kappa) \cos(\pi w_p \kappa_x) \cos(\pi w_p \kappa_y)}{\widehat{S}(0)}. \tag{28}$$

Eq. (24) and (28) are the two formulas which relate the LGS image shape S to the mean-square subaperture tilt measurement error due to noise.

A finer point is that the measurement errors due to noise in the x- and y-components of the tilt estimate will be correlated for those subapertures where the elongation of the LGS is not parallel to either the x or y axis. For completeness, the covariance of the two estimation errors is given by

$$\langle (\theta_x - \vartheta_x)(\theta_y - \vartheta_y) \rangle = \left(\frac{\partial \Delta_x}{\partial \theta_x} \right)^{-1} \left(\frac{\partial \Delta_y}{\partial \theta_y} \right)^{-1} \frac{f'}{(f\bar{N})^2}, \tag{29}$$

where the quantity f' is defined by the expression

$$\begin{aligned} f' &= \frac{\bar{N}_1 - \bar{N}_2 + \bar{N}_3 - \bar{N}_4}{\bar{N}} \\ &= \frac{-4 \int d\kappa \, \widehat{S}(\kappa) \widehat{D}(\kappa) \sin(\pi w_p \kappa_x) \sin(\pi w_p \kappa_y)}{\widehat{S}(0)}. \end{aligned} \tag{30}$$

3.2 Sample Numerical Results

This subsection summarizes sample numerical results on variations in quadrant detector gain as a function of various LGS and AO system parameters. Similar results are presented for f, the fraction of the total signal received by the WFS subaperture which is incident on the quad cell. The parameters used for these calculations are as follows:

- 0.589 μm laser wavelength (λ);
- Sodium layer altitude of 95 ± 5 km;
- Zenith angles of 0 and 45 degrees;
- 4 meter separation in x between the laser launch telescope and the WFS subaperture (d_s);
- 0.45 meter laser launch telescope diameter (d_T);
- 0.30 meter laser beam diameter with a beam quality of 1.0 or 1.5 (BQ);
- $r_0 = 0.16$ m at zenith and 0.5 microns;
- 0.5 or 0.67 meter subaperture width (w_R)
- 0.5 to 1.5 arc sec pixel width in the WFS camera (w_p);
- WFS lenslet blurring of the LGS image by $0.25\lambda/w_R$; and

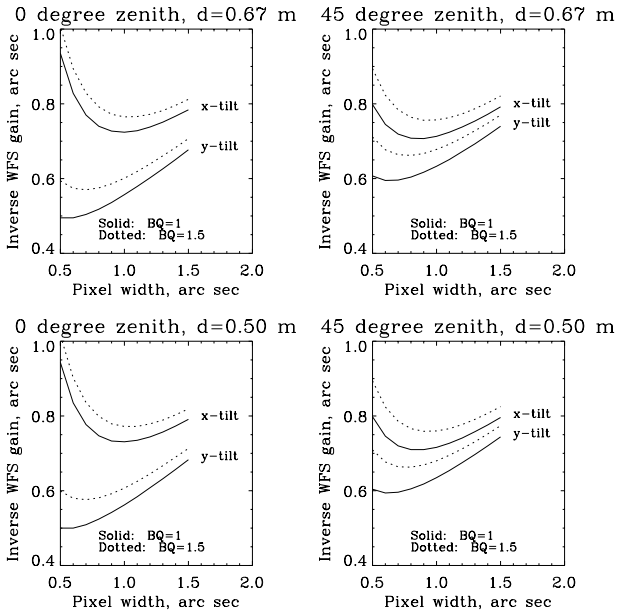

Figure 1: Inverse quadrant detector gain vs pixel size

For a fixed signal-to-noise ratio, the RMS tilt estimation error for a Shack-Hartmann WFS is proportional to the inverse of the quadrant detector gain with respect to tilt. The atmospheric and AO parameters used for these calculations are listed in the text.

- CCD pixel crosstalk blurring of the LGS image by $0.25 w_p$.

Results are plotted as a function of the pixel width w_p, since we are interested in optimizing the angular width of the pixels in the WFS camera.

Fig. 1 plots the *inverse* of the quadrant detector gain $\partial\Delta/\partial\theta$ as a function of WFS pixel size for laser beam qualities of 1.0 and 1.5, WFS subaperture widths of 0.5 and 0.67 meters, and zenith angles of 0 and 45 degress. By Eq. (23), the RMS tilt estimation error due to noise is equal to this inverse gain times the RMS variability in the qual cell energy imbalance Δ_x. The difference in results for the x- and y-dimensions is due to the elongation of the LGS. For small pixel sizes the quadrant detector gain decreases (and the inverse of the gain increases) due to the truncation of the LGS image by the quad cell. For large pixel sizes, the quadrant detector gain decreases due to the increased blurring of the LGS image by detector crosstalk. Degrading the laser beam quality from 1.0 to 1.5 increases the inverse quadrant detector gain by about 0.05 arc seconds. The inverse quadrant detector gain is minimized for pixel sizes between about 0.8 to 1.0 arc seconds, with performance degrading more rapidly as pixel size is decreased.

Fig. 2 plots analogous results for the faction f of the LGS image incident on the quadrant detector. This quantity is about 80 per cent for a 1 arc second pixel, and relatively insensitive to variations in beam quality. Based upon the results in these two figures, a WFS pixel width of 1 arc second has been used to estimate and optimize LGS AO performance as a function of LGS signal level.

4 LGS AO Performance Optimization vs LGS Signal Level

Using the LGS noise model developed in the preceeding two sections, LGS AO and MCAO performance can now be evaluated as a function of LGS signal level. The analysis code used for this purpose is essentially the same as used earlier to evaluate Altair and other systems, and has been described previously [4, 5]. Of course, AO system performance depends upon the control algorithm as well as the LGS signal level, and at

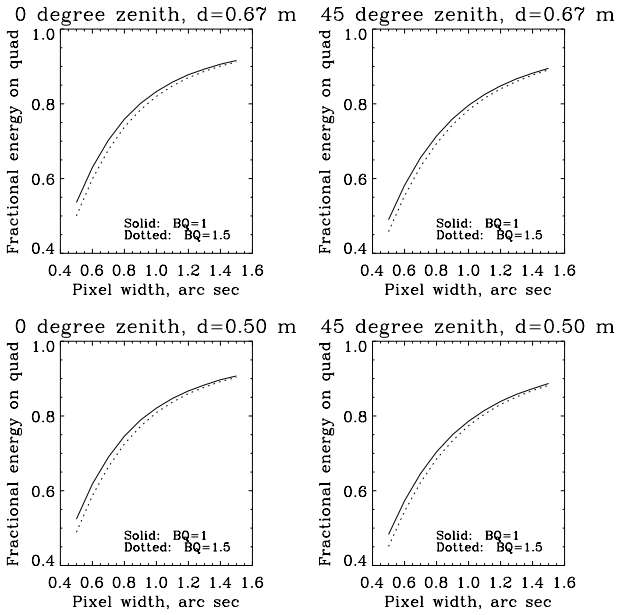

Figure 2: Fraction of LGS signal incident on a quad cell vs. pixel size

For a fixed total LGS signal level, increasing the fraction f of the signal incident on a quad cell improves tilt estimation accuracy according to Eq.'s (23) and (27). The parameters used for these calculations are the same as for Fig. 1.

least some parameters of the algorithm must be adjusted as a function of signal level to achieve satisfactory performance. For this analysis, the approach to optimizing the AO control algorithm is as follows:

- Define a scenario in terms of zenith angle (0 or 45 degrees), seeing (50 or 20 per cent Cerro Pachon profiles), atmospheric wind profile (median Cerro Pachon profile), WFS subaperture width (0.5 or 0.67 meters), detector read noise (4, 6, or 9 electrons), laser beam quality (1.5), and WFS pixel angular subtense (1.0 arc seconds). The remaining parameters of the LGS noise model are fixed, with values as specified in Section 3 above. Tables 1 and 2 summarize the atmospheric profiles used for these calculations.

- Vary the LGS WFS signal level at zenith from 12 to 500 PDE's/cm^2/sec. The signal level for the same LGS is reduced by a factor of 0.64 at a zenith angle of 45 degrees, due to the increased air mass and the increased range to the sodium layer. The laser powers corresponding to these LGS signal levels are summarized in Section 6 below.

- For each LGS signal level, vary the WFS sampling rate from 200 to 1000 Hz to optimize AO system performance in terms of the short exposure (tilt-removed) Strehl ratio in H band. AO control loop gain (0.5), detector read noise, and AO control loop latency (2 processing cycles total) are held fixed independent of sampling rate, so that optimum AO performance at low LGS signal levels may be slightly underestimated. The wave-front reconstruction matrix is reoptimized for each LGS signal level and WFS sampling rate using "binary modal control," with all wavefront modes controlled at a gain of either 0.5 or 0.0 (i.e., not controlled at all).

Due to the large number of cases considered, it is impractical to follow this prescription for MCAO. AO control loop bandwidth and performance have been optimized as a function of LGS signal level for a conventional LGS AO system. MCAO results for a reduced range of LGS signal levels, using control bandwidths as optimized for the conventional LGS AO system, are summarized in Section 5 below.

The optimized Strehl ratios for the conventional LGS AO case are plotted in Fig.'s 3–6 for the 50 and 20 per cent Cerro Pachon turbulence profiles and zenith angles of 0 and 45 degrees. Each figure plots tilt-

Relative Altitude, km	Relative C_n^2	Windspeed, m/sec
0.0	0.647	6.7
1.8	0.080	8.3
3.3	0.119	13.4
5.8	0.035	25.6
7.4	0.025	33.9
13.1	0.080	22.2
15.8	0.015	8.9

Table 1: Discretized $C_n^2(h)$ and windspeed profiles for 50 per cent seeing at Cerro Pachon

This is a seven-layer fit to a mean 50 per cent profile computed from SCIDAR and thermosond measurements at Cerro Pachon. Altitudes are given relative to the altitude of the site. The $C_n^2(h)$ values are expressed as a fraction of the total integrated strength of C_n^2, which corresponds to an r_0 of 0.166 meters at a wavelength of 0.5 microns.

Relative Altitude, km	Relative C_n^2	Windspeed, m/sec
0.0	0.676	6.6
1.6	0.070	8.0
3.1	0.108	12.4
5.3	0.027	23.2
7.4	0.032	33.7
13.1	0.086	22.2

Table 2: Discretized $C_n^2(h)$ and windspeed profiles for 20 per cent seeing at Cerro Pachon

These values are analogous to Table 1, except they are a fit to a mean 20 per cent profile at Cerro Pachon. The corresponding r_0 is 0.210 meters at 0.5 microns.

removed Strehl ratios in J, H, and K bands vs LGS signal level for AO systems of order 12 by 12 and 16 by 16, with either 4, 6, or 9 electrons of detector read noise. The corresponding tilt-removed Strehl ratios with no measurement noise and an infinite control bandwidth are listed in Table 3 for comparison. In general the curves do not contain sharp break points, so it is difficult to define a firm requirement for LGS signal level. A specification of about 80 PDE's/cm^2/sec appears to be a reasonable minimum, however. At this signal level the H band Strehl ratio due to the combined effects of noise and servo lag is 0.95 for average seeing and a zero degree zenith angle. For J band the Strehl ratio due to these effects is 0.91, which increases to 0.93 [0.95] with 125 [200] photodetection events. These last three values also describe performance in H band at a 45 degree zenith angle. The optimized WFS sampling rates for these cases range from about 500 to 800 Hz, but the performance variations with sampling rate and control bandwidth are very slight due to the tradeoff between servo lag and noise gain. The variations in performance between 4 and 6 noise electrons per pixel per read in the WFS camera are also very modest, with more appreciable penalties for 9 noise electrons.

Finally, a requirement to adjust the WFS sampling rate as a function of zenith angle and seeing may increase the cost and complexity of a pulsed laser system. For such a laser, it may be desirable to instead adjust the control loop bandwidth by varying loop gain at a fixed WFS sampling rate. This will increase the penalty associated with detector read noise, but will also help to improve performance by decreasing the latency in the control loop. Such higher-order effects are beyond the scope of the current analysis.

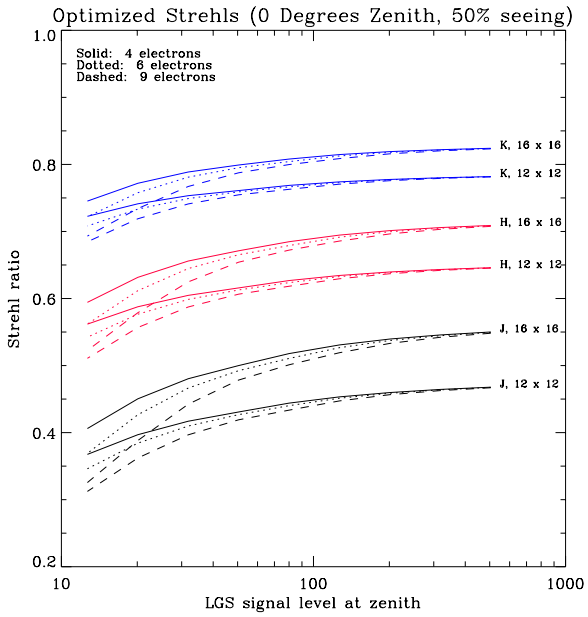

Figure 3: LGS AO performance vs LGS signal level (50% seeing, 0 degree zenith)

This figure plots short-exposure (tilt removed) Strehl ratios in J, H, and K bands for AO systems with 12 by 12 and 16 by 16 WFS subapertures. The LGS signal level is described in terms of WFS photodetection events per square centimeter of collecting area per second. Refer to the text for descriptions of the other system parameters and the AO control algorithm.

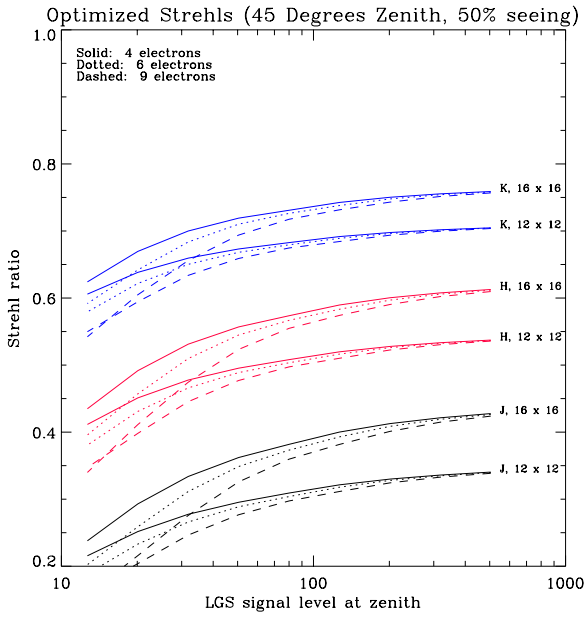

Figure 4: LGS AO performance vs LGS signal level (50% seeing, 45 degree zenith)

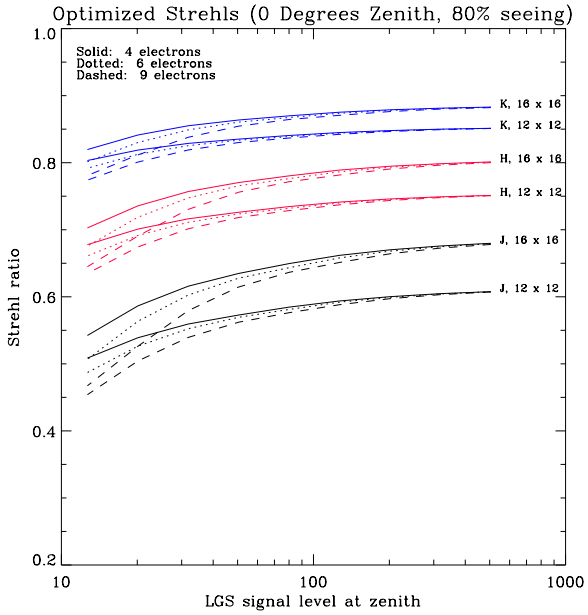

Figure 5: LGS AO performance vs LGS signal level (20% seeing, 0 degree zenith)

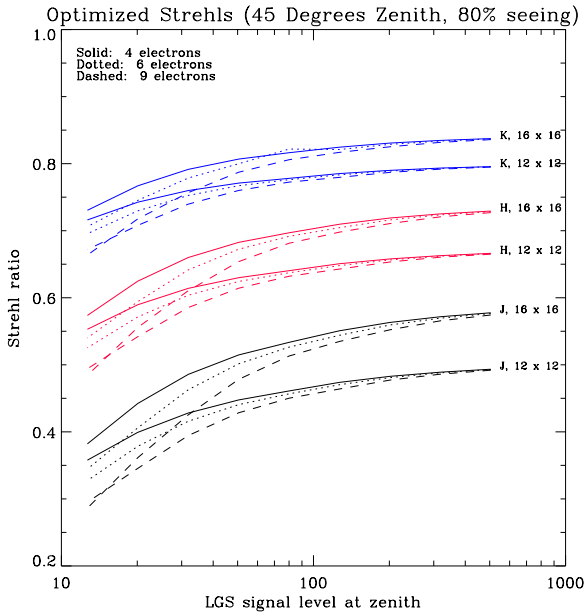

Figure 6: LGS AO performance vs LGS signal level (20% seeing, 45 degree zenith)

N_{sa}	Seeing	ψ, degrees	Strehl Ratio		
			J	H	K
12	50%	00	0.481425	0.656808	0.789301
12	50%	45	0.356750	0.552154	0.715694
12	20%	00	0.620850	0.760519	0.857213
12	20%	45	0.510026	0.679076	0.804279
16	50%	00	0.568429	0.722350	0.832718
16	50%	45	0.451144	0.631792	0.771921
16	20%	00	0.695826	0.811903	0.889516
16	20%	45	0.599394	0.744859	0.847278

Table 3: LGS AO Strehl ratios without WFS noise or servo lag

N_{sa} is the number of WFS subapertures across the WFS pupil, and the 50% and 20% seeing values refer the to C_n^2 profiles listed in Tables 1 and 2.

5 MCAO Results

Because of the increased number of WFS subapertures and DM actuators, the computation requirements to evaluate Strehl ratios as a function of LGS signal level and WFS sampling rate are much larger for MCAO than for conventional LGS AO with a single guide star. We have not been able to evaluate MCAO performance for as wide a range of LGS signal levels or rigorously optimize the WFS sampling rates. Fig.'s 7 and 8 illustrate a more limited set of results computed for (i) average seeing conditions, (ii) 16 by 16 subapertures per WFS, (iii) LGS signal levels of 80, 125, and 200 photodetecton events/cm^2/sec, and (iv) WFS sampling rates derived from the LGS AO analysis in section 4. The estimated Strehl ratio reductions for a given LGS signal level are more significant for MCAO than for LGS AO. For example, the Strehl reduction in H band for 80 PDE's/cm^2/sec at a zero degree zenith angle is a factor of 0.91 at the center of the field and 0.85 at the corner of the field, compared to a factor of 0.93 for conventional LGS AO. For 200 PDE's/cm^2/sec the corresponding values are 0.95, 0.90, and 0.97. The results are similar in J band and at a 45 degree zenith angle–the Strehl ratio reduction due to WFS noise at the center of the MCAO field is a few per cent worse than for conventional LGS AO, with the size of the reduction increasing with distance off-axis. Even with this increased sensitivity to noise, LGS signal levels in the range of 80 to 200 PDE's/cm^2/sec provide a reasonably uniform level of correction over a field-of-view much larger than provided by conventional AO.

Heuristically, this increased sensitivity to noise for MCAO may arise from the need to invert the cross-coupled influence of multiple deformable mirrors upon multiple wave front sensors. Some improvement can be obtained by optimizing the AO control loop bandwidth and possibly by reducing the number of WFS subapertures. This will be investigated after the *NGS* signal requirements for MCAO have been evaluated.

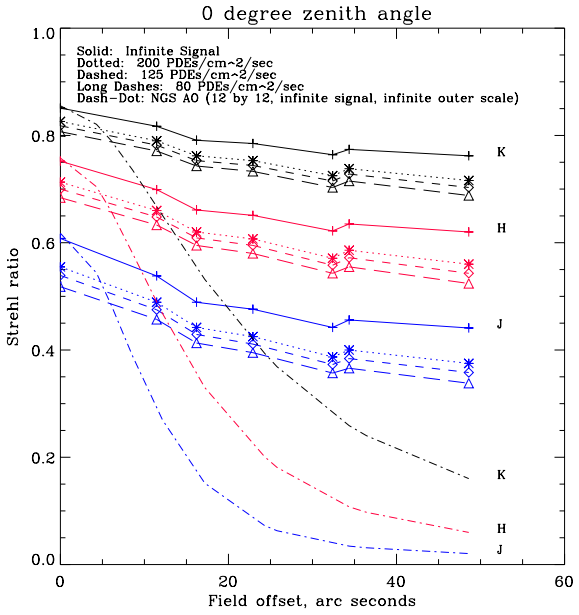

Figure 7: MCAO performance vs LGS signal level (50% seeing, 0 degree zenith)

These results are for a system with 16 subapertures across each WFS pupil and 6 read noise electrons. The remaining parameters for the LGS noise model are the same as listed in section 3 above. The Strehl ratios for a noise-free NGS AO system with 12 by 12 subapertures are plotted for comparison.

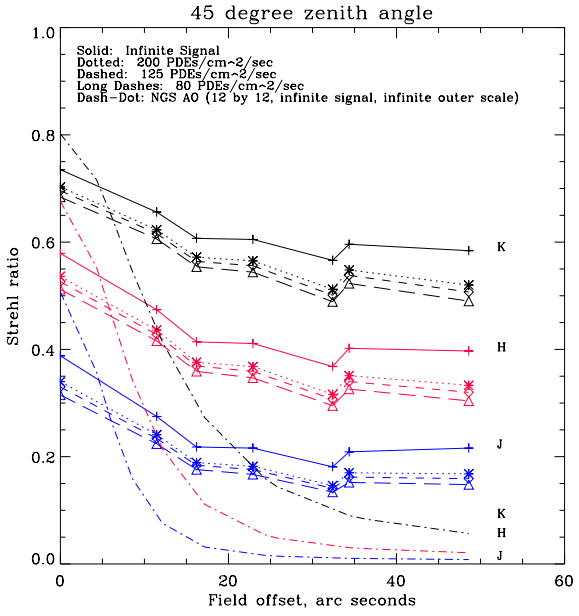

Figure 8: MCAO performance vs LGS signal level (50% seeing, 45 degree zenith)

Apart from the zenith angle, these results are analogous to those in fig. 7.

6 Laser Power Requirements

This section briefly reviews the relationship between LGS laser source power and the LGS WFS signal level, and summarizes the power requirements for three sample lasers to deliver WFS signal levels of 80 to 200 PDE's/cm^2/sec. As presented earlier [1], the WFS signal level is related to laser power by the equations

$$N_{\rm det} = T_R \eta N_{\rm col} \tag{31}$$

$$N_{\rm col} = P_L T_L \cdot {\rm SE} \cdot (C_s \sec\psi)(T^{\sec\psi})^2/(H \sec\psi)^2, \tag{32}$$

where:

- $N_{\rm det}$ is the LGS WFS signal level (80, 125, or 200 photodetection events/cm^2/sec for these calculations),
- T_R is the optical transmittance through the telescope and WFS optics on the receive path (0.49),
- η is the detector quantum efficiency (0.85),
- $N_{\rm col}$ is the LGS signal level at the telescope primary mirror,
- P_L is the laser power in watts (laser-dependent, to be deterined as a function of $N_{\rm det}$),
- T_L is the optical transmittance on the laser launch path (dependent upon laser location),
- SE is the unsaturated slope efficiency, which is proportional to the cross section of a sodium atom (dependent upon laser pulse format),
- C_s is the column density of the sodium layer (2×10^9 atoms/cm^2),
- ψ is the zenith angle (zero degrees),
- T is one-way atmospheric transmittance at zenith (0.90, corresponding to 0.12 magnitudes per air mass), and
- H is the altitude of the sodium layer (90 km).

These parameter values are the same as used previously, except that T has been increased from 0.8 to 0.9 after a review of atmospheric transmittance data for Mauna Kea [6]. The sodium laser column density C_s varies seasonally, and the value used here is near the low end of the annual range.

Eq.'s (31) and (32) can be used to determine the laser power required to achieve a specified LGS WFS signal level $N_{\rm det}$. Table 6 presents results for $N_{\rm det}$ = 80, 125, and 200. Three previously described laser formats are considered, referred to here as CW, long pulse, and macro-micro pulse [1]. The laser power requirements for $N_{\rm det}$ = 125 and 200 are approximately equal to the requirements and goals specified in the MK LGS laser system RFP.

References

[1] C. d'Orgeville, M. R. Chun, J. Sebag, C. Boyer, D. Montgomery, J. M. Oschmann, F. Rigaut, and D. Simons, "Gemini Mauna Kea Laser Guide Star System," *SPIE Proc.* **3762**, [3762-21], (1999).

[2] F. Rigaut, B. L. Ellerbroek, and M. J. Northcott, "Comparison of curvature-based and Shack-Hartmann-based adaptive optics for the Gemini Telescope," Appl. Opt., **36**, 2856–68, (1997).

[3] S. Morris, "Calculation of Optimal Pixel Scale for Altair (including bad lenslet blur)", 1998.

[4] B. L. Ellerbroek and D. W. Tyler, "Adaptive optics sky coverage calculations for the Gemini-North Telescope," Proc. Ast. Soc. Pac., **110**, 165–85, 1998.

Laser format		CW	Long pulse	Macro/micro pulse
Slope efficiency, SE		0.26	0.10	0.33
Launch transmittance, T_L		0.54	0.72	0.72
Laser power, Watts	$N_{\rm det} = 80$	6.9	13.5	4.1
	$N_{\rm det} = 125$	10.9	21.3	6.1
	$N_{\rm det} = 200$	17.3	33.7	10.2

Table 4: Laser power requirements vs LGS WFS signal level

This table summarizes laser power requirements computed using Eq.'s (31) and (32). The quantities SE, T_L, and $N_{\rm det}$ are defined in the text.

[5] B. L. Ellerbroek, "First-order performance evaluation of adaptive-optics systems for atmospheric turbulence compensation in extended-field-of-view astronomical telescopes," J. Opt. Soc. Am A **11**, 783–805 (1994).

[6] CFHT Extinction curve for Mauna Kea, http://www.cfht.hawaii.edu.